Research Square

Preprints are preliminary reports that have not undergone peer review.
They should not be considered conclusive, used to inform clinical practice,
or referenced by the media as validated information.

Research on the Mechanical Behavior and Damage Constitutive Model of Fractured Sandstone Constrained by CFRP

Lei Chen

cd9194198420163.com

Liaoning Technical University

Taiyu Liu

Liaoning Technical University

Jiaxu Jin

Liaoning Technical University

Shuguang Zhang

Guangxi Key Lab. of Geomechanics and Geotechnical Engineering

Baoxin Jia

Liaoning Technical University

Jiashun Liu

Liaoning Technical University

Jupeng Tang

Shenyang University

Research Article

Keywords: Anchored rock mass, Fissured sandstone, CFRP constrained, Energy evolution, Damage constitutive model

Posted Date: November 11th, 2026

DOI: https://doi.org/10.21203/rs.3.rs-9810348/v1

License: This work is licensed under a Creative Commons Attribution 4.0 International License.
Read Full License

Additional Declarations: No competing interests reported.

Research on the Mechanical Behavior and Damage Constitutive Model of Fractured Sandstone Constrained by CFRP

Lei Chen[1,2,3,4*], Taiyu Liu[2], Jiaxu Jin[2] , Shuguang Zhang[5], Baoxin Jia[2,3,4], Jiashun Liu[2], Jupeng Tang[6]

[1] *School of Mechanics and Engineering, Liaoning Technical University, Fuxin 123000, ,Liaoning, China*

[2] *School of Civil Engineering, Liaoning Technical University, Fuxin 123000 Liaoning, China*

[3] *Ordos Institute of Liaoning Technical University, Ordos 017004, Inner Mongolia, China*

[4] *Key Laboratory of Disaster Management and Ecological Restoration in Resource-depleted Mining areas of Liaoning Province, Fuxin 123000 Liaoning, China*

[5] *Guangxi Key Lab. of Geomechanics and Geotechnical Engineering, Guilin 541004, Guangxi, China*

[6] *School of Environmental Science, Shenyang University, Shenyang 110044, Liaoning, China*

Correspondent: Lei Chen, E-mail: cd919419842@163.com

Abstract: Aiming at the engineering problem of the coordinated deformation and failure of the advanced support structure of deep roadways and the overburden fissured rock mass, taking the transportation roadway of the 40101 mining face of Gaojialiang Coal Mine in Ordos as the engineering background, a flexible support structure formed by the simulation of surrounding rock and advanced support using carbon fiber reinforced composite material (CFRP) is adopted. The mechanical response, failure mode and energy damage evolution mechanism of fissured sandstone under different CFRP constrained areas and fissure angles are studied through a uniaxial compression test. The results show that as the constrained areas of CFRP gradually increases, the peak strength, elastic modulus and peak strain of fissured sandstone gradually increase, the Poisson's ratio gradually decreases, the failure mode gradually changes from brittle split failure to ductile shear failure, the energy storage capacity increases, the critical threshold for the conversion from elastic energy to dissipated energy gradually moves backward, and the initial stress level of damage significantly increases. The mechanical parameters exhibit significant anisotropy with the fissure angle. The peak strength, elastic modulus and peak strain all show an asymmetric "V" shaped evolution pattern with the fissure angle, with the minimum values all located at θ=45°, and the Poisson's ratio monotonically increases with the fissure angle. Based on fracture mechanics and statistical damage theory, the CFRP constraint coefficient β was introduced to modify the stress intensity factor K_I at the fissure tip. A damage constitutive model of sandstone with prefabricated fissures considering the modification of CFRP constraints was established. The accuracy and rationality of the model were verified in combination with the test results. The research results provide a reliable theoretical basis for the collaborative design of fissure surrounding rock and advanced support in deep roadways.

Key words: Anchored rock mass, Fissured sandstone, CFRP constrained, Energy evolution, Damage constitutive model

Article Highlights:(1)Using carbon fiber reinforced polymer (CFRP) to simulate the flexible reinforced zone formed by forepoling support and surrounding rock provides a new experimental

approach.(2)It reveals that CFRP confinement can effectively suppress the radial deformation of rock, changing its failure mode from brittle splitting to ductile shear.(3)It has been clarified that CFRP confinement enhances the energy storage capacity of rock and significantly delays the critical threshold at which elastic energy is converted into dissipated energy.(4)By introducing the CFRP constraint coefficient to modify the stress intensity factor, a constitutive model of fractured sandstone damage was developed that can accurately reflect experimental patterns.

1. Introduction

With the continuous increase in the depth of coal and mineral resource exploitation, the geological environment faced by deep underground projects is becoming increasingly complex (Liu et al.,2026). Under the combined effects of high ground stress (Ling et al.,2026) and strong mining-induced disturbances and fracture water (Deng et al.,2026), the surrounding rock of the roadway often exhibits significant nonlinear and large deformation and rheological characteristics, posing severe challenges to the control of the roadway surrounding rock (Zhang et al.,2026). Especially for the widely distributed fissured sandstone formations, due to the presence of primary fissures within the rock mass or secondary fissures induced by excavation, the integrity of the rock mass is compromised and the mechanical strength is significantly reduced (Liu et al.,2026;Sun et al.,2024). During the excavation process, the fissured sandstone is highly prone to expansion, sliding and deformation (Xie et al.,2025;Zhang et al.,2026). Therefore, revealing the mechanism of the coordinated deformation and failure of the fractured surrounding rock and the advanced support during the roadway excavation process holds significant theoretical and engineering significance.

In terms of CFRP reinforcement structures, the existing research mainly focus on the study of fissured rock masses, concrete components, and their reinforcement performance and damage evolution mechanisms in complex environments (Pi et al.,2025). Using CFRP to simulate the reinforcement structure, a graded loading rheological test was conducted on fissured sandstone to reveal the aging deformation mechanism of fissured rock under CFRP reinforcement (Zhang et al.,2022). For recoverable seismic-resistant structures, a new type of detachable and recyclable CFRP-steel fiber reinforced concrete composite column is proposed. Through the collaborative method of indoor tests and numerical simulations, the enhancement mechanisms of the low damage, high energy dissipation and recoverable seismic resistance performance of the composite column due to the fiber volume ratio, axial compression ratio and strength grade are clarified, and a damage theoretical model is established (Liu et al.,2025). Under the coupling condition of Marine corrosion and fatigue, the recovery ability of CFRP plate spined anchorage system to the bearing capacity of degraded reinforced concrete beam and its performance deterioration mechanism are revealed (Zhou et al.,2025). Based on the real-time monitoring technology of four-point bending loading - acoustic emission (AE) and machine learning algorithms such as GMM-SVM and DTW-DBA-K-means, the interaction mechanism of CFRP layers and reinforcement ratio on the evolution path and failure mode of flexural and tensile damage of coral sand reinforced concrete beams, the microcrack early warning mechanism and the optimal reinforcement scheme were revealed (Wang et al.,2025) The dual reinforcement method of

ultra-high performance concrete (UHPC) coating and near-surface embedded CFRP bars was adopted to enhance the bending and shear resistance of lightweight reinforced concrete beams, reveal the optimal ductility mechanism of split precast slabs, and establish a strength prediction model (Willy et al.,2025) . Through the combined analysis method of fracture mechanics tests and AE monitoring, the influence laws of CFRP layers and the prestress level on the fissure parameters and damage evolution process of concrete beams with cracks were analyzed (Liu et al.,2025). Through cyclic torsion tests and finite element methods, the torsional failure mechanism of rectangular hollow reinforced concrete columns reinforced with CFRP and glass fiber composites was revealed, and an interface damage constitutive model considering hysteresis mechanical characteristics was established (Zhang et al.,2024). In terms of rock mass mechanics for anchoring, the shear mechanical characteristics of rock joints under different anchoring lengths were discussed. The influence law of anchoring length on the shear strength of joints and the shear resistance behavior of anchor rods were analyzed (Zhang et al.,2024). Through indoor tests and numerical simulation methods, the regulation mechanism of shear strength by the lateral restraint of anchor rods was revealed, and a mechanical model of anchor rods that simultaneously considers the combined action of axial tension and lateral shear was established (Wei et al.,2024). For the anchoring system composed of anchor rods, anchor cables and rock masses, the mechanism by which the two work together to resist the release of energy from dynamic disasters was explored (Wang et al.,2023). Based on the fracture mechanics, the differential equation of interfacial shear stress for rock beams anchored with static fissures is established, and the distribution laws of interfacial stress and axial force between anchor rods and surrounding rock in the disturbance area at the fracture tip are analyzed (Ning et al.,2025). By three-point bending tests and numerical simulation methods, the distribution laws of anchorage position and preloading level on the fissure toughness, fracture energy and stress concentration at the fracture tip of fissured rock mass are clarified, effectively enhancing the fissure toughness of rock mass (Su et al.,2024).

In conclusion, the existing research has revealed the deformation laws of the surrounding rock of deep roadway fissures and initially clarified the failure mechanism of the anchored rock mass under uniaxial compression. However, the research on the combined deformation and failure characteristics of anchored fissured rock mass and advanced support is relatively limited (Song et al.,2026). Based on the summary of existing achievements, this paper uses CFRP to simulate the flexible support structure formed by grouting anchor rods and surrounding rock. By conducting uniaxial compression tests, the stress-strain relationship and failure mode of sandstone under different constraint areas and fissure angles are obtained. Based on the energy theory, the energy evolution law of fissured sandstone under the constraint of CFRP is analyzed. Furthermore, a damage constitutive model of sandstone with prefabricated fissures considering the constraint modification of CFRP is established, and the model is verified with the test data. This further revealed the collaborative deformation and failure mechanism of deep roadway surrounding rock and advanced support, with the aim of providing a theoretical basis for the anchoring support design of deep roadway surrounding rock.

2. Experiment Introduction

2.1 Proposal of CFRP circumferential constraint idea

The surrounding rock of deep roadways is usually in a complex stress environment. As

shown in Fig.1, during the excavation of the roadway, the surrounding rock is disturbed by the excavation, and the original stress balance state is disrupted. Therefore, effective structural constraints need to be applied to restrict the protrusion and deformation of the surrounding rock towards the open surface. Before the excavation of the working face, it is usually necessary to carry out advanced support for the surrounding rock, that is, the control measures taken to ensure the stability of the upper surrounding rock after the excavation of the lower surrounding rock. The commonly used forms of advanced support at present include advanced anchor rods, pipe sheds, advanced small pipe grouting and advanced horizontal rotary jet grouting, etc. Among them, the advanced anchor rod are widely used in roadway construction due to their convenient and good support effect. Its mechanism is to drive the anchor rods into the rock layer along the direction of excavation. Through the bonding force and friction between the anchor rods and the rock mass, a flexible reinforcement zone is formed, thereby improving the stress concentration phenomenon of the surrounding rock after excavation (Jorge Terron-Almenara et al.,2025). After the rock mass beneath the anchor rods support is excavated, the rock mass above the anchor rods undergoes downward displacement due to the gravity, and the flexible reinforcement zone formed together with the anchor rods and the surrounding rock undergoes coordinated deformation. Therefore, this paper intends to use CFRP, a common material in engineering, to constrain standard rock specimens, in order to approximately simulate the flexible reinforcement zone formed by advanced anchoring support and surrounding rock, providing reliable theoretical support for further in-depth research on the mechanical response of deep roadway surrounding rock under effective structural constraints and its cooperative deformation mechanism. The research results have certain theoretical significance.

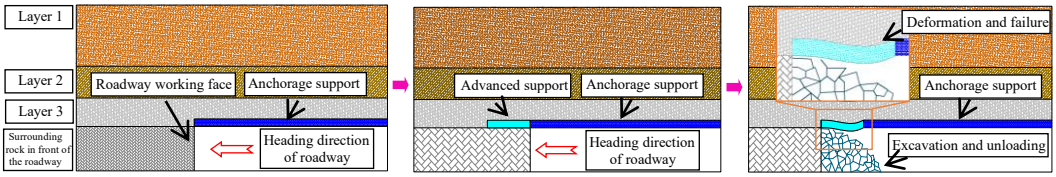


Fig.1. Schematic diagram of coordinated deformation and failure of surrounding rock and advanced support.

2.2 Specimen preparation and testing equipment

The sandstone used in the test is taken from the roof of the transportation tunnel of the 40101 mining face of Gaojialiang Coal Mine. The sandstone in this mining area is gray in its natural state, with uniform grains and no macroscopic visible joints or fissures on the surface. According to the rock mechanics test method recommended by the International Society for Rock Mechanics (ISRM), natural rock blocks are processed into standard cylindrical specimens with a diameter of 50 mm and a height of 100 mm. The deviation of the straightness should be less than 0.05 mm, and the deviation of height and diameter should be less than 0.3 mm. The initial physical parameters are shown in Fig. 2. To avoid significant differences in the test results, all specimens are taken from the same intact rock block, and wave velocity tests are conducted on all specimens, and specimens with large differences are excluded.

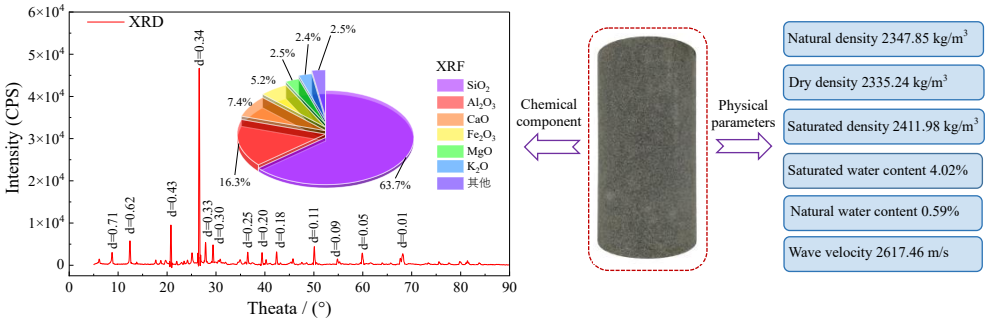


Fig.2. Sandstone mineral composition.

Before the indoor tests, the mineral composition and chemical composition of sandstone are detected by using the TTR-III X-ray diffractometer from Japan and the Panalytical Axios X-ray fluorescence spectrometer from Netherlands. The results are shown in Fig. 2. The main chemical composition in this paper includes SiO_2(63.7%), Al_2O_3(16.3%), CaO(7.4%), Fe_2O_3(5.2%), MgO(2.5%) and K_2O(2.4%). To obtain sandstone specimens with different fissure angles, high-pressure water jets are used to cut the complete specimens. The fissure are 20 mm long and 1 mm high, with fissure angles of θ=0°, θ=30°, θ=45°, θ=60° and θ=90° respectively. The prepared fissure sandstone are shown in Fig. 3.

The uniaxial compression test is completed on the fully automatic rock mechanics test system independently developed by the Institute of Rock and Soil Mechanics, Chinese Academy of Sciences, Wuhan, as shown in Fig. 3. The maximum axial force of this system is 2000 kN, the maximum confining pressure is 60 MPa, the maximum osmotic pressure is 60 MPa, the maximum dynamic disturbance force is 500 kN, the frequency is 0 to 10 Hz, the maximum temperature is 150℃, and the minimum temperature is -20℃. The axial deformation is measured by an LVDT displacement sensor. The above parameters meet the test requirements of this paper.

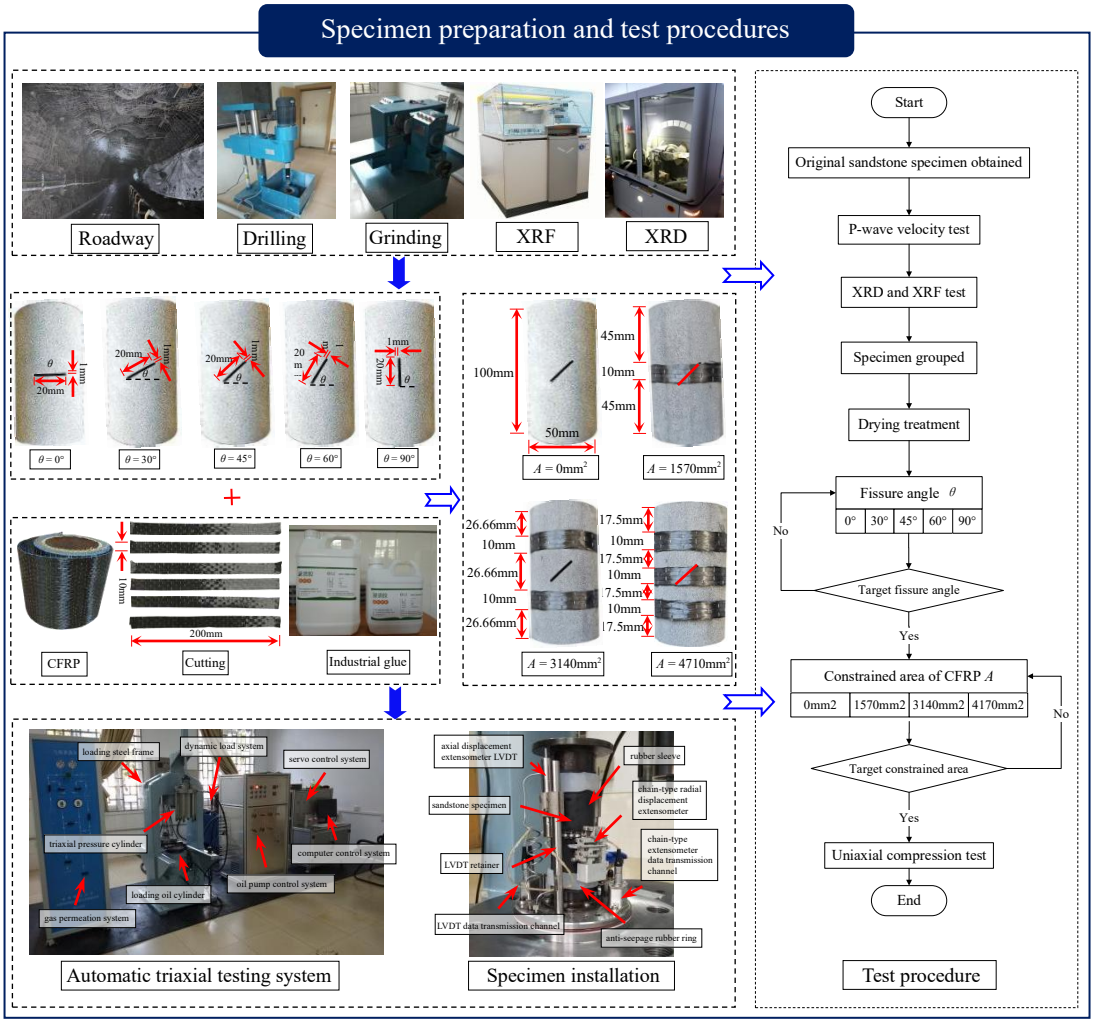


Fig. 3. Specimen preparation and test procedures.

2.3 Test methods and procedures

To study the deformation and failure characteristics of the surrounding rock of deep roadways under effective structural constraints, this paper intends to use CFRP to approximately simulate the flexible reinforcement zone jointly formed by advanced support and surrounding rock. The preparation process of CFRP-constrained fissured sandstone is as follows.

(1) The fissured sandstone is dried at a temperature of 104℃ for 24 hours. After drying, the specimens are taken out and cooled to room temperature.

(2) Cutting the CFRP into rectangular strips that are 10 mm wide and 200 mm long, with the length slightly longer than the circumference of the cylinder, to facilitate the impregnation adhesive bonding.

(3) Prepare the main agent and curing agent in the impregnating adhesive in a ratio of 2:1, stir evenly with an electric mixer, and let it stand at room temperature for 1h to ensure that the main agent and curing agent can fully react and maximize the bonding strength of the impregnating adhesive.

(4) Evenly apply the prepared impregnating adhesive on the CFRP, and then adhere it to the surface of the specimens in sequence according to the test scheme in Fig. 3. The adhered specimens need to be placed at room temperature for 48 hours to ensure that the CFRP can fully bond with the fissured sandstone.

Based on the research results of Chen et al.(Chen et al.,2022) , in this paper, the constrained

areas of fissured sandstone are set as A=0mm^2, A=1570mm^2, A=3140mm^2 and A=4710mm^2 respectively, as shown in Fig. 3. Three parallel tests are conducted for each working condition to ensure the reliability and repeatability of the test results. The technical parameters of CFRP and industrial impregnating adhesive are shown in Table 1, and the entire test process is presented in Fig. 3. The uniaxial compression test adopts the displacement control loading method, with the loading rate set at 0.05 mm/min until the instability and failure end. Stress-strain data and failure characteristics are obtained simultaneously.

Table 1 Technical parameters of CFRP and industrial glue

CFRP			Industrial glue		
Project	Parameter		Project		Parameter
Strength grad	High-strength Class I	High-strength Class II	Mechanical Properties	Tensile strength / MPa	≥38
Unit weight / (g/m^2)	300	200		Tensile elastic modulus / MPa	≥2400
Theoretical thickness / mm	0.167	0.111		Elongation / %	≥1.5
Standard value of tensile strength / MPa	≥3400	≥3000		Bending strength / MPa	≥50
Modulus of tensile elasticity / GPa	≥230	≥200		Compressive strength / MPa	70
Rate of elongation / %	≥1.6	≥1.5	Adhesive property	Tensile strength / MPa	≥38
Bending strength / MPa	≥700	≥600		Tensile elastic modulus / MPa	≥2400
Interlaminar shear strength / MPa	≥45	≥35		Elongation / %	≥1.5
Length deviation	±1.5%			Bending strength / MPa	≥50
Width deviation	±0.5%				
Mass deviation per unit area	±3.0%			Compressive strength / MPa	70

3. Analysis of Test Results of CFRP-constrained Fissured sandstone

3.1 Analysis of stress-strain curve

Under the action of external forces, the stress-strain curve of rocks can reflect the entire process from the sealing of internal micro-defects, the propagation and penetration of new cracks, to instability and failure. The uniaxial compressive stress-strain curves of sandstone under different CFRP constraint areas and fissure angles are shown in Fig. 4. The variation trends of the uniaxial compressive stress-strain curves of sandstone under different test conditions are generally similar, all having gone through the crack compaction stage, elastic deformation stage, plastic yield stage and post-peak strain softening stage. Under the same fissure angle, the peak strength, peak strain and elastic modulus of the specimens gradually increase with the constraint area, becoming more obvious in the compaction section. The nonlinear characteristics of the stress-strain curve gradually intensify. Moreover, as the constraint area gradually increases, the post-peak curve of some specimens shows a "stepped" stress drop, and the failure mode gradually changes from brittle to plastic. There are obvious differences from the brittle failure mode of unconstrained specimens. The reason is that the circumferential constraint provided by CFRP effectively enhances the mechanical properties of fissured sandstone. By restricting radial

deformation, the specimen can still maintain a certain load-bearing capacity in the post-peak stage. The sliding gnawing effect at the failure surface causes the post-peak curve to drop in a "stepped" manner. When the loading reaches the tensile ultimate strength of CFRP, the constraint fails and the specimen undergoes unstable failure. Under the same constrained area, the peak strength, peak strain and elastic modulus of the specimen all show a trend of first decreasing and then increasing with the increase of the fissure angle. The Poisson's ratio gradually increases, and no obvious changes occur in the compaction stage and the plastic yield stage.

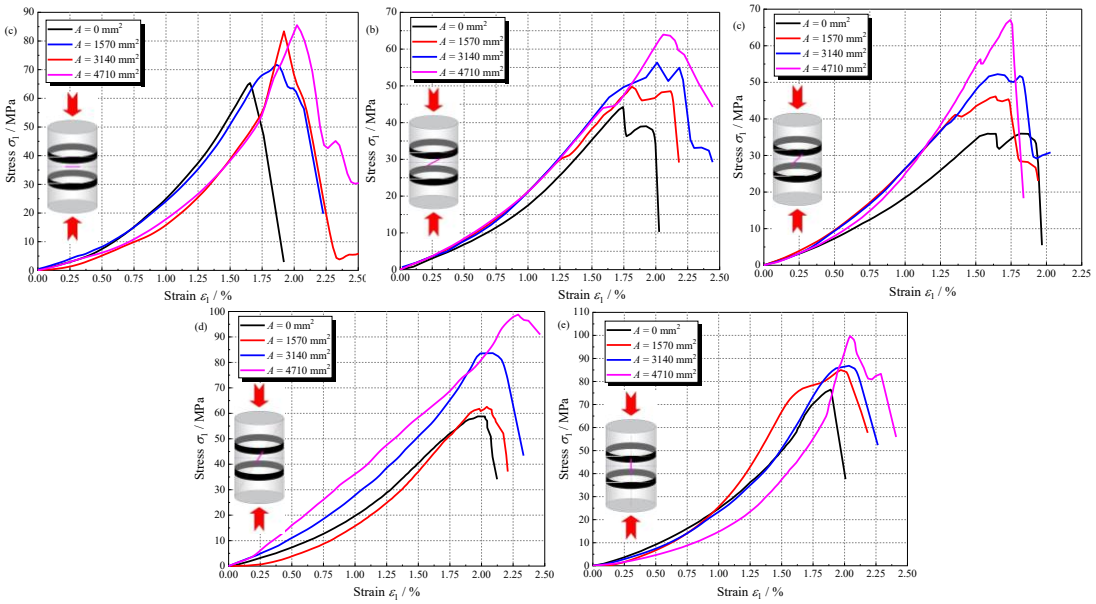


Fig.4. Stress-strain curve of CFRP constrained fissured sandstone. (a) θ=0°; (b) θ=30°; (c) θ=45°; (d) θ=60°; (e) θ=90°.

3.2. Analysis of mechanical parameters

The strength, strain, elastic modulus and Poisson's ratio of rocks are the four most fundamental parameters in rock mechanics and also the four most important indicators for evaluating the failure capacity of rock masses. To quantitatively analyze the influence of CFRP constraint and fissure angle on the mechanical properties of sandstone, the mechanical parameters are obtained based on the stress-strain curve. Table 2 shows the mechanical parameters with different fissure angles. The mechanical parameters of sandstone under different test conditions are shown in Fig. 5, and the variation curves of each parameter with the CFRP constrained areas and the fissure angles are presented in Fig. 6.

Table 2 Mechanical parameters of fissured sandstone under different test conditions

CFRP constrained areas A / mm²	Mechanical parameters				
	Fissure angle θ / (°)	Peak strength σ_{pk} / MPa	Peak strain ε_{pk} / %	Elastic modulus E / GPa	Possion's ratio μ
1570	0°	71.69	0.186	26.17	0.198
	30°	50.22	0.187	22.99	0.199
	45°	46.15	0.164	22.04	0.201
	60°	62.74	0.205	24.63	0.203
	90°	85.06	0.202	29.26	0.205

It can be seen from Fig. 5 and Fig. 6 that under the same fissure angle, as the CFRP constraint area increases, the peak strength, elastic modulus and peak strain of the sandstone gradually increase, while the Poisson's ratio gradually decreases. Under the same CFRP

constrained area, as the fissure angle gradually increases, the peak strength, elastic modulus and peak strain of sandstone all show a trend of first decreasing and then increasing, and the minimum values all occur at the fissure angle $\theta = 45°$.

The essence of rock failure lies in the initiation, propagation and penetration of internal microcracks. Under the constraint of CFRP, the damage evolution path of rocks changes. When there is no of CFRP, under the axial load, tensioning wing cracks are prone to occur at the tips of fissure in rocks. The propagation direction of such wing cracks is controlled by the direction of the maximum principal stress, causing significant radial expansion and volume expansion of the rock, and ultimately inducing brittle splitting failure. The bearing capacity under this failure mode is relatively low. After applying the constraint of CFRP, it is equivalent to providing passive lateral constraint stress to the rock, thereby inhibiting the propagation of cracks and delaying the accumulation of damage. As the constraint area of CFRP increases, the lateral constraint force gradually increases. According to the Mohr-Coulomb strength criterion $\tau=\tau_0+\sigma_n\tan\varphi$, the increase in lateral constraint significantly raises the normal stress σ_n on the fissure surface, thereby enhancing the shear strength τ. Rocks need to reach a higher load level to overcome the CFRP constraint effect and achieve shear zone penetration. In addition, the larger the constraint area is, the more significant the effect of inhibiting crack propagation and delaying damage evolution will be.

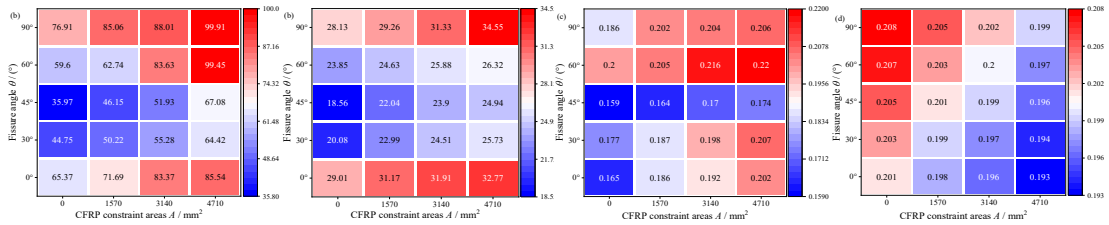


Fig.5. Hot spot diagrams of mechanical parameters of fissured sandstone under different test conditions: (a) Peak strength σ_{pk}; (b) Elastic modulus E; (c) Peak strain ε_{pk} / %; (d) Possion's ratio.

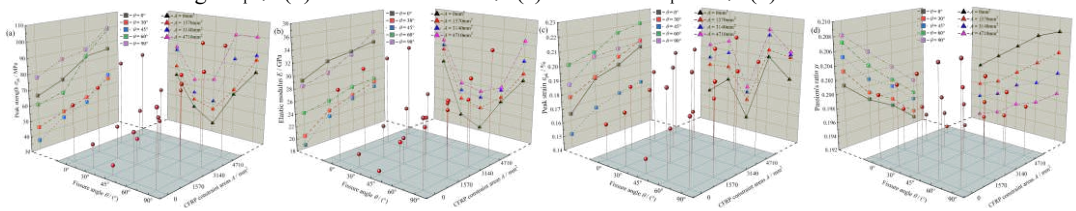


Fig.6. Distribution law of mechanical parameters of fissured sandstone under different test conditions : (a) Peak strength σ_{pk}; (b) Elastic modulus E; (c) Peak strain ε_{pk} / %; (d) Possion's ratio.

Regarding the influence of fissure angle, according to the Mohr-Coulomb theory, the shear stress τ acting on the fissure surface is $\tau=0.5(\sigma_1-\sigma_3)\sin2\theta$, and the normal stress σ_n is $\sigma_n=0.5[(\sigma_1+\sigma_3)+(\sigma_1-\sigma_3)\cos2\theta$. When $\theta=45°$, the shear stress τ approaches its maximum value, while the normal stress σ_n is moderate. At this point, it is conducive to overcoming the internal friction Angle and cohesion of the fissure surface, resulting in the sliding failure of the fissure surface and the poorest mechanical properties. When $\theta<45°$, the fissure surface is nearly parallel to the direction of the principal stress, and the failure needs to penetrate the rock matrix or form new wing cracks, with a relatively high bearing capacity. When $\theta>45°$, the crack surface is nearly perpendicular to the direction of the principal stress. At this time, the crack is closed under pressure, and the shear stress is very small. The failure is mainly manifested as compression-shear or tensioning at the crack tip, and a greater load is required to cause failure.

To make a more intuitive comparison of the differences in the mechanical parameters of sandstone under different CFRP constraint areas and fissure angles, the evolution laws of each

parameter are drawn as shown in Fig. 7. Under the condition of fissure angle θ=45°, when the constrained areas A = 0 mm^2, the peak strength of the specimen is 35.97 MPa, the peak strain is 0.159%, the elastic modulus is 18.56 GPa, and the Poisson's ratio is 0.205. When the constrained areas of CFRP are A=1570 mm^2, A=3140 mm^2 and A=4710 mm^2 respectively, compared with A=0 mm^2, the peak strengths increased by 28.3%, 44.37% and 86.48% respectively. The elastic modulus increased by 18.75%, 28.77% and 34.38% respectively, the peak strain increased by 3.14%, 6.92% and 9.43% respectively, and the Poisson's ratio decreased by 1.95%, 2.92% and 4.39% respectively. Under the condition that the constrained areas A = 3140 mm^2, when the fissure angle θ=45°, the peak strength is 51.93 MPa, the peak strain is 0.170%, the elastic modulus is 23.9GPa, and the Poisson's ratio is 0.196. When the fissure angles are θ=0°, 30°, 60° and 90° respectively, compared with θ=45°, the peak strength increased by 60.54%, 6.45%, 61.04% and 69.48% respectively, and the elastic modulus increased by 30.42%, 2.55%, 8.28% and 31.09% respectively. The peak strain increased by 12.94%, 16.47% and 27.06%, 20.0% respectively, and the Poisson's ratio increased by 0.51%, 1.53%, 2.04% and 3.06% respectively. The CFRP constrained areas and fissure angle have a significant influence on the mechanical properties of rocks.

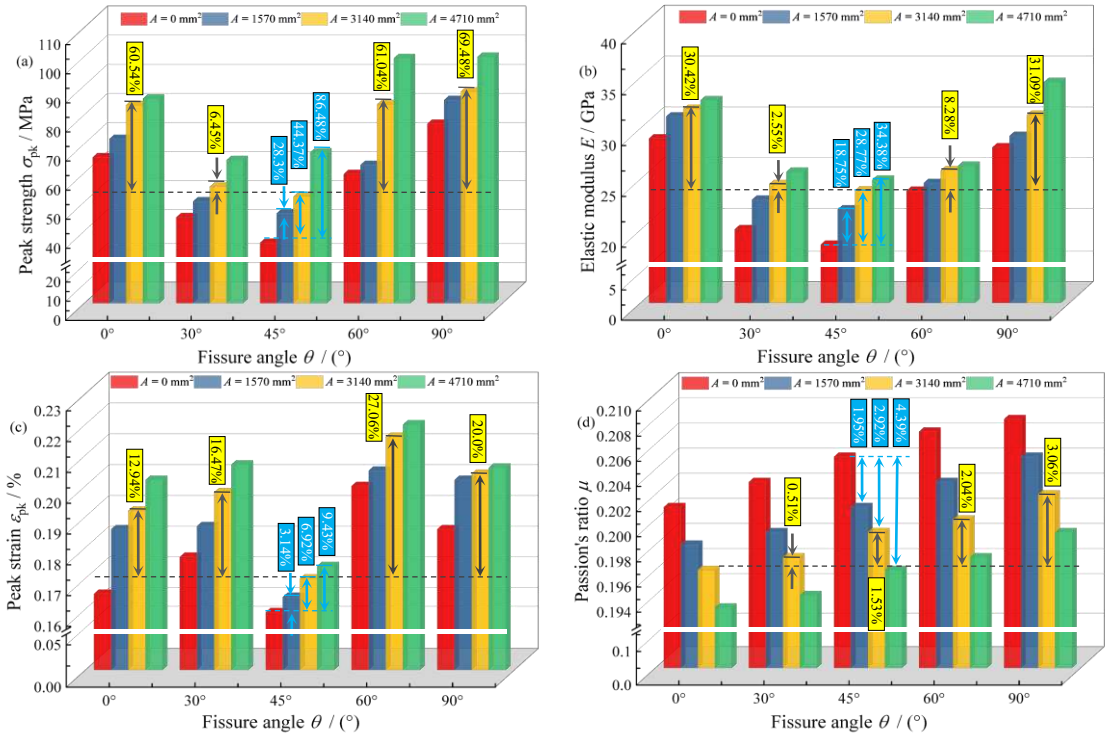


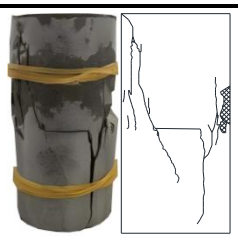
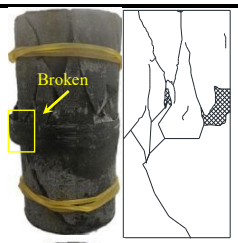
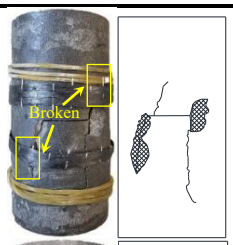
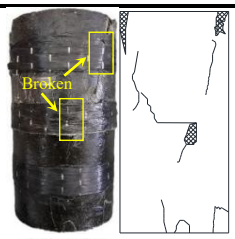
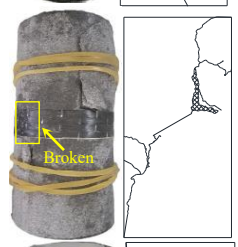
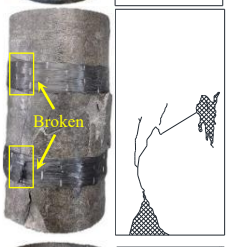
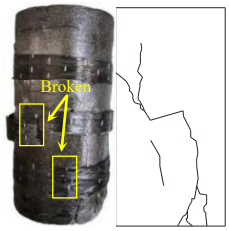
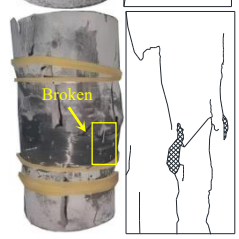
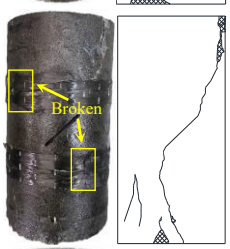
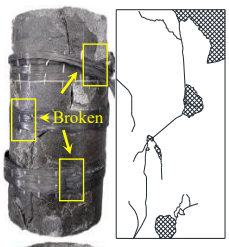
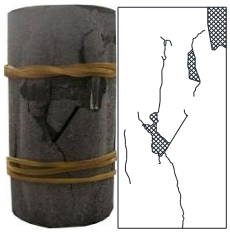
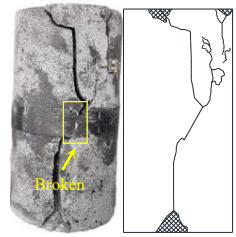
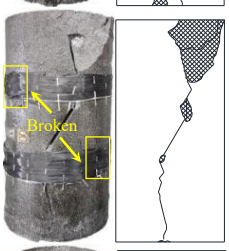
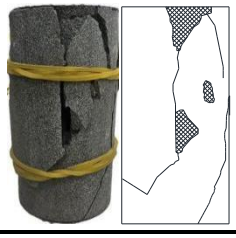
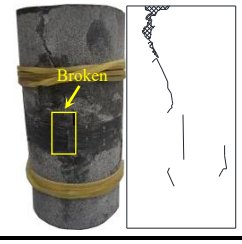
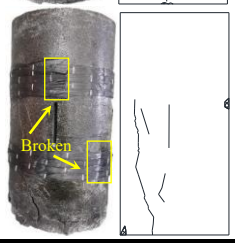
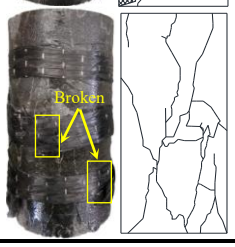
Fig. 7. Response laws of mechanical parameters of fissured sandstone under different test conditions: (a) Peak strength σ_{pk}; (b) Elastic modulus E; (c) Peak strain ε_{pk} / %; (d) Possion's ratio.

3.3 Analysis of Damage Characteristics

The failure modes of sandstone under different CFRP constraint areas and fissure angles are shown in Table 3. The specimen is severely broken at the tip of the prefabricated fissure. As the constrained area of CFRP gradually increases, the failure mode of fissured sandstone gradually changes from brittle splitting failure to ductile shear failure. When the constrained areas are A=3140mm^2 and A=4710mm^2, CFRP effectively suppressed the radial deformation of the specimen, causing the internal cracks to evolve from a single wing crack propagation to a mixed propagation form of multiple microcracks. The reason for the above phenomenon can be

explained that the stress concentration is prone to occur at the fissure tip, giving rise to tip wing cracks and reverse wing cracks. The area near the fissure is prone to damage due to the associated effect of crack propagation. After being constrained by CFRP, the radial deformation of the specimen is suppressed, and the crack propagation path changes. As the constrained area of CFRP gradually increases, the provided constrained strength significantly improves, effectively suppressing the tensile stress concentration at the fissure tip and enhancing the bearing capacity of the sandstone.

Table 3 Failure modes of fissured sandstone under different test conditions

Fissure angle θ	CFRP constraint areas A / mm^2			
	0	1570	3140	4710
0°				
30°				
45°				
60°				
90°				

From the perspective of energy dissipation, under the constraint of CFRP, the surface of the specimens all showed varying degrees of fragmentation. The reason can be explained that the stress concentration in the constraint areas of CFRP, which led to significant compressive fragmentation in the local compression area. The dissipated energy of rocks is mainly released through the closure of internal micro-cracks and crack propagation. Among them, the energy consumed by tensile crack propagation is smaller than that of shear crack propagation, so

secondary cracks are easily induced at the tip of wing cracks, thereby releasing the accumulated dissipated energy. When the elastic strain energy stored inside the specimen exceeds the dissipated energy, its surface will release the energy by forming macroscopic fragmentation. Table 3 presents the broken positions of CFRP when it reaches the tensile strength. At the moment of CFRP broken, the binding force suddenly disappears, and the elastic energy accumulated inside the specimen is rapidly released. For fissured sandstonewith different CFRP confined areas, the larger the constrained area, the more energy is stored inside the specimen, the more energy release after instability, and the more severe the CFRP broken.

4. Analysis of Energy Evolution Law of Fissured Sandstone Constrained by CFRP

4.1 Principle of Energy calculation

The essence of rock deformation and failure is a dynamic transformation process of energy absorption, storage, dissipation and release (Gu et al.,2026) . When the rock is subjected to external load, part of the energy is stored in the rock in the form of elastic energy, and the other part is dissipated through plastic deformation and damage evolution. When the elastic energy absorbed and stored by the rock from the external load reaches its energy storage limit, instantaneous instability failure will occur. At this point, part of the stored strain energy is converted into the surface energy of the newly fissured surface, while the rest of the energy is released to the external system in the form of kinetic energy, thermal energy and radiant energy of the failure rock mass. To explore the energy damage evolution mechanism during the deformation and failure process of fissured rock masses. The energy dissipation evolution laws of sandstone under different fissure angles and different CFRP constraint areas are analyzed, with the aim of revealing the mechanical response and failure mechanism of rock masses during loading from an energy perspective. Fig. 8 shows the basic principle of calculating the energy of rocks per unit volume and the division of energy stages.

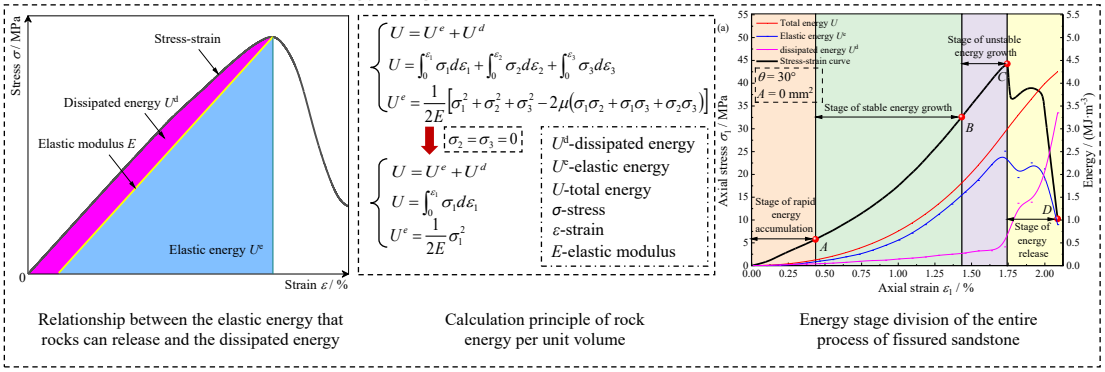


Fig.8. Basic principles of calculating rock energy per unit volume and the energy evolution curve.

Taking the test conditions of θ = 30° and A = 0mm^2 as an example (Fig. 8), the energy evolution throughout the whole process of loading can be roughly divided into four stages.

(1) Stage of rapid energy accumulation (OA): This stage corresponds to the linear elastic deformation stage of the rock, and point A corresponds to the cracking stress. External load is converted into energy absorbed by the rock and stored in the form of elastic energy. The elastic energy curve shows a "concave" growth trend. At this stage, almost no energy dissipation occurs,

and the total energy is equal to the elastic energy, with the dissipated energy approaching zero.

(2) Stage of stable energy growth (AB): This stage corresponds to the stable propagation stage of rock cracks, and point B corresponds to the expansion stress. The external load is continuously converted into energy absorbed by the rock, and the elastic energy approximately shows a linear growth trend. At this stage, new cracks begin to form inside the rock, causing the dissipated energy to increase slowly.

(3) Stage of unstable energy growth (BC): This stage corresponds to the unstable propagation stage of rock cracks, and point C corresponds to the peak strength. At this stage, internal cracks in the rock expand rapidly. The elastic energy curve changes from linear growth to "convex" growth, while the dissipated energy curve is exactly the opposite, changing from linear growth to "concave" growth, and the proportion of dissipated energy gradually increases.

(4) Stage of energy release (CD): This stage corresponds to the post-peak failure stage of rocks, where internal cracks in the rocks rapidly expand and penetrate, forming macroscopic fractures. At this stage, the elastic energy curve drops rapidly. After the elastic energy is released, it is converted into dissipated energy, and then the dissipated energy curve increases sharply, while the total energy remains basically unchanged.

4.2 Analysis of energy evolution characteristics

Based on the principle of rock energy calculation, taking the fissure angle θ=30° as an example, the energy evolution curves of sandstone under different constraint areas are shown in Fig. 9. The energy evolution laws of fissured sandstone with different CFRP constrained areas are relatively similar. At the initial stage of loading, the total energy U continues to accumulate. The variation trend of the elastic energy U^{e} is consistent with that of the total energy, and both increase synchronously. The dissipated energy U^{d} increases slowly. When the specimen reaches its peak strength, the elastic energy U^{e} also reaches its maximum value. Along with the instability failure of the specimen, the elastic energy U^{e} is rapidly released, the curve drops, and the growth rate of the dissipated energy U^{d} significantly accelerates until the end of the test.

At different energy evolution stages, the CFRP constraint effect has a significant impact on the energy accumulation and dissipation characteristics of rocks. During the stage of rapid energy accumulation, the total energy U and elastic energy U^{e} show a nonlinear and slow growth trend, and the dissipated energy U^{d} approaches zero. This stage is mainly characterized by the compression sealing of microcracks and primary defects within the sandstone, and the constraint effect of CFRP is not yet significant. After entering the stage of stable energy growth, the total energy U and elastic energy U^{e} increase linearly. CFRP begins to play the role of "passive confining pressure", significantly enhancing the energy storage capacity. Moreover, the larger the constraint area of CFRP, the stronger the energy storage capacity and the higher the accumulation of elastic energy. As the axial load continues to increase, the specimen enters a stage of unstable energy growth. Under the constraint of CFRP, the difference between the total energy U and the elastic energy U^{e} gradually expands, but the pre-peak dissipated energy U^{d} still remains at a relatively low level, indicating that the CFRP constraint effectively delays the internal damage evolution process of the sandstone. After entering the energy release stage, the specimen constrained by CFRP still maintain a certain bearing capacity after the peak, indicating that CFRP constraint effectively suppresses the instantaneous and intense release of energy, promoting the transformation of the rock failure mode from brittle to ductile.

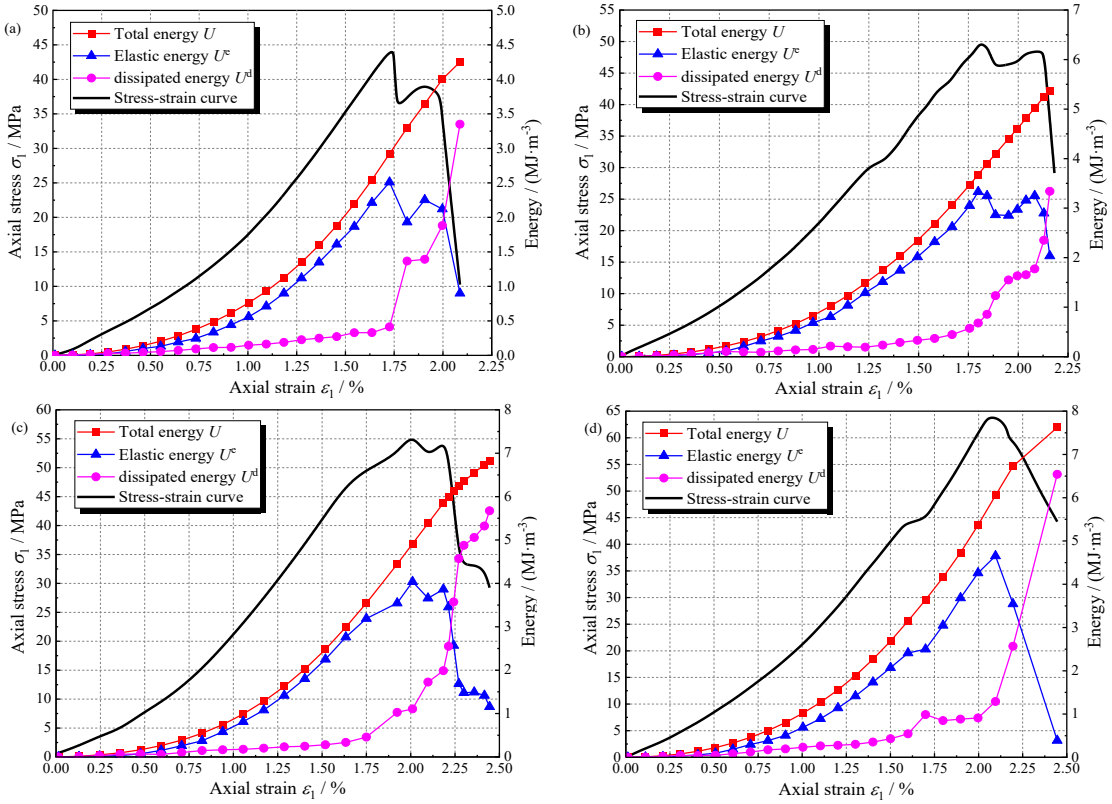


Fig.9. Energy evolution curves of fissured sandstone under different constrained areas (θ=30°)：(a) A=0mm^2; (b) A=1570mm^2; (c) A=3140mm^2; (d) A=4710mm^2.

To further analyze the energy proportion of fissured sandstone under different CFRP constrained areas, based on the energy evolution curve in Fig. 9, the energy proportions of before failure under different CFRP constrained areas with a fissure angle of θ = 30° are extracted as shown in Fig. 10, and σ_{ci}, σ_{cd}, and σ_{pk} represent the rock initiation stress, expansion stress, and peak strength, respectively (Zhang et al.,2025). Under different CFRP constraint areas, as the axial load gradually increases, the proportion of dissipated energy gradually increases. When the CFRP constrained area is A=0mm^2, the proportions of dissipated energy at the characteristic stress points are 1.97%, 6.68% and 11.97% respectively. When the CFRP constrained area is A=1570mm^2, the proportions of dissipated energy are 2.45%, 7.16% and 12.22% respectively. When the CFRP constrained area increased to A=4710mm^2, the proportions of dissipated energy are 2.68%, 8.44% and 14.13% respectively. The increase in the CFRP constrained area leads to a gradual increase in the proportion of dissipated energy. The reasons have been given in the previous text and will not be elaborated here.

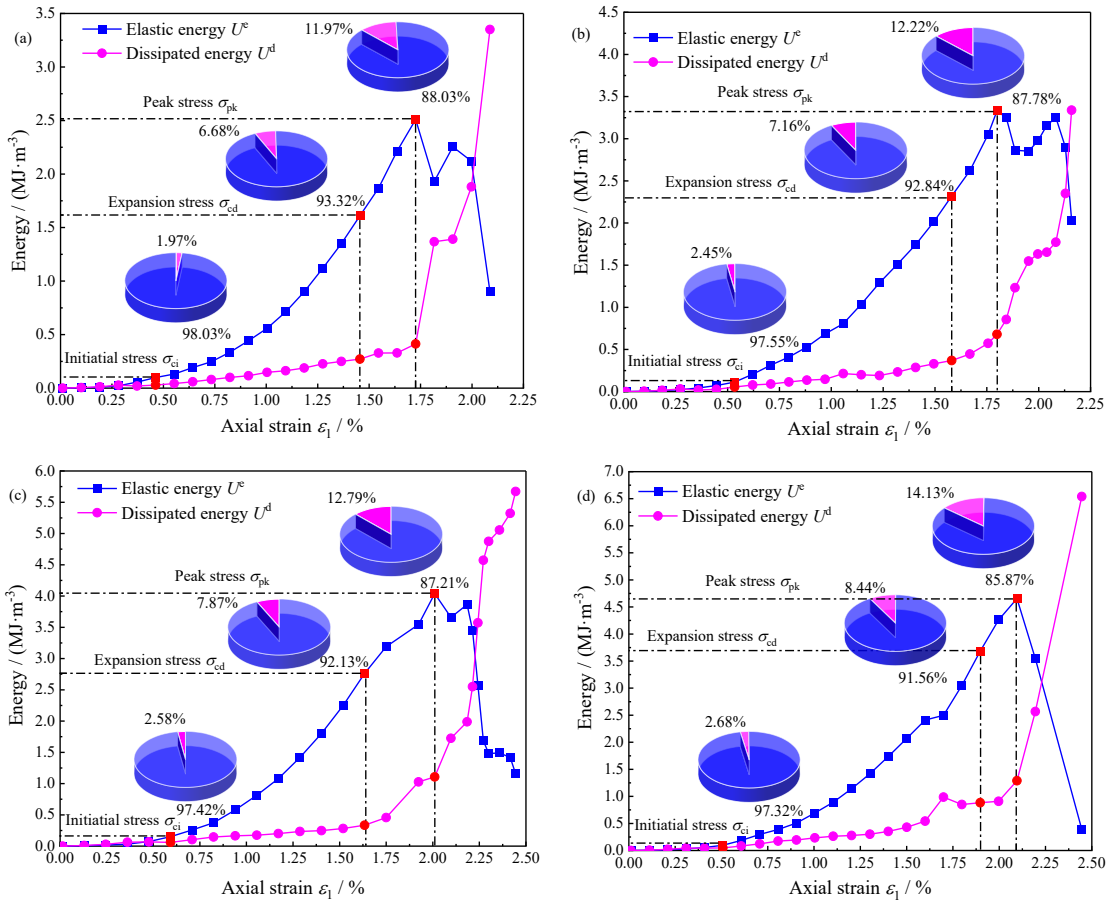


Fig.10. Energy proportion of fissured sandstone under different constrained areas (θ=30°)：(a) A=0mm^2; (b) A=1570mm^2; (c) A=3140mm^2; (d) A=4710mm^2.

To comparatively analyze the influence of the variation of CFRP constrained area on the energy evolution law of fissured sandstone, the evolution curves of total energy, elastic energy and dissipated energy under different CFRP constrained areas are extracted and shown in Fig. 11. As the CFRP constrained area gradually increases, the total energy and elastic energy corresponding to the same axial strain gradually increase, while the dissipated energy gradually decreases. Among them, the total energy reflects the total work done by external forces on the rock, demonstrating the overall energy absorption capacity of the rock. The increase in the CFRP constrained area significantly enhances the energy absorption performance of the rock, endowing the originally brittle sandstone with higher energy absorption toughness, thereby effectively delaying the occurrence of macroscopic failure. Elastic energy is the releaseable energy accumulated within rocks, which directly affects the energy storage characteristics and instability mechanism of rocks. The increase of the CFRP constraint area will significantly enhance the elastic energy, indicating that the constraint effect improves the energy storage capacity of fissured sandstone and delays the critical state of the conversion of elastic energy to dissipated energy. Dissipated energy is mainly used for frictional sliding at the fissure surface, the initiation and propagation of microcracks, and is a key parameter characterizing the internal damage evolution process of rocks. With the increase of the CFRP constraint area, the growth of the dissipated energy curve tends to flatten, indicating that the constraint effect effectively inhibits the development of cracks and significantly increases the initial stress level of damage at the same time.

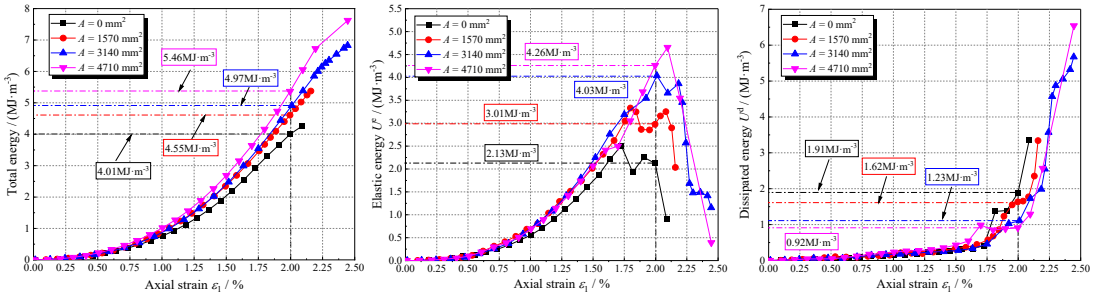


Fig.11. Comparison of energy evolution of fissured sandstone with different constrained areas (θ = 30°).

The dissipated energy, elastic energy and total energy corresponding to the peak strength of fissured sandstone under different CFRP constraint areas are obtained according to Fig. 11, as shown in Fig. 12. When the CFRP constraint area is A=0mm^2, the total energy at its peak strength is 3.65MJ·m^{-3}, the elastic energy is 2.25MJ·m^{-3}, and the dissipation energy is 1.39MJ·m^{-3}. When the CFRP constraint area are A=1570mm^2, A=3140mm^2 and A=4710mm^2 respectively, compared with A=0mm^2, the total energy increased by 9.86%, 41.1% and 62.7% respectively, and the elastic energy increased by 48.0%, 79.6% and 106.7% respectively, and the dissipated energy reduced by 51.1%, 20.1% and 7.2% respectively. The above data indicates that all three kinds of energy are significantly affected by the CFRP constraint area, and when the constraint area is A=1570mm^2, the elastic energy and the dissipated energy are the most sensitive.

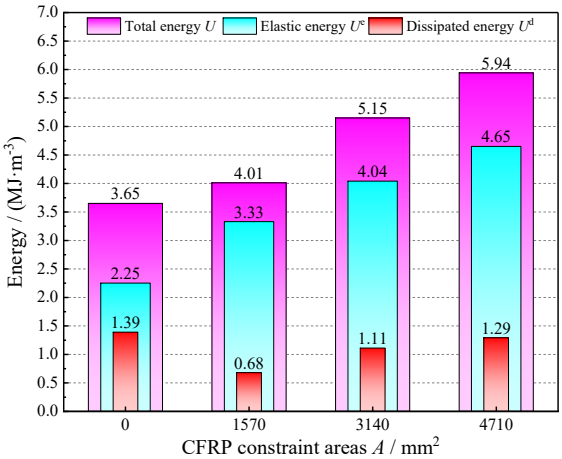


Fig.12. Statistical results of energy at peak strength.

5. Establishment of a constitutive model for damage of fissured sandstone constrained by CFRP

5.1 Damage variables under loading

The interior of rocks contains a large number of randomly microscopic defects. It is assumed that these microscopic defects follow certain distribution characteristics. Based on the theory of statistical damage, the Weibull function is used to describe the distribution characteristics of micro-element strength(WEIBULL W et al.,1951). The probability density function $P(f)$ can be expressed as:

$$P(f)=\frac{m}{f_0}\left(\frac{f}{f_0}\right)^{m-1}\exp\left[-\left(\frac{f}{f_0}\right)^{m}\right] \tag{1}$$

Where f is the random variable of the strength of micro-elements; m and F_0 are Weibull parameters, which respectively reflect the dispersion of internal defects in rocks and the average strength of micro-elements.

Assuming the number of micro-elements inside the rock is N_t and the number of micro-elements failure by loading is N_f, then the loading statistical damage variable D_m can be expressed as:

$$D_m = \frac{N_f}{N_t} \tag{2}$$

The number of micro-elements failure by loading N_f can be expressed as:

$$N_f = \int_0^f N_t P(f) df \tag{3}$$

Taking the micro-element strength as the damage evolution variable, by combining (1), (2), and (3), the expression of the load statistical damage variable D_m can be expressed as:

$$D_m = 1 - \exp\left[-\left(\frac{f}{f_0} \right)^m \right] \tag{4}$$

Assuming that the rock exhibits isotropy under uniaxial compression, based on Lemaitre's equivalent strain principle (Lemaitre J et al.,2012), the initial damage constitutive model of fissured sandstone can be expressed as:

$$\sigma_1 = E_1 \varepsilon_1 (1 - D_m) = E_1 \varepsilon_1 \exp\left[-\left(\frac{f}{f_0} \right)^m \right] \tag{5}$$

Where σ_1 is the axial stress, MPa; ε_1 is the axial strain; E_1 is the elastic modulus, GPa.

Based on the D-P criterion (Alcazar E et al.,2025), the distribution variable of the micro-element strength can be expressed as:

$$f = \alpha_0 I_1 + \sqrt{J_2} \tag{6}$$

Where α_0 is the internal friction Angle coefficient of the rock; I_1 is the first invariant of the stress tensor; J_2 is the second invariant of the stress bias tensor. And the three parameters can be respectively expressed as:

$$I_1 = \sigma_1, \quad J_2 = \frac{\sigma_1^2}{3}, \quad \alpha_0 = \frac{\sin\varphi}{\sqrt{9 + 3\sin^2\varphi}} \tag{7}$$

Where φ is the internal friction Angle of the sandstone, °.

Combining equations (6) and (7):

$$f = \frac{\sigma_1}{\sqrt{3}} \left(1 + \frac{\sin\varphi}{\sqrt{3 + \sin^2\varphi}} \right) \tag{8}$$

The stress-strain curve must satisfy the following boundary conditions at its peak strength:

(a) When $\varepsilon = \varepsilon_{pk}$, then $\sigma = \sigma_{pk}$, where σ_{pk} and ε_{pk} are the peak strength and peak strain, respectively.

(b) When $\varepsilon = \varepsilon_{pk}$, then $d\sigma/d\varepsilon = 0$.

Based on the above boundary conditions, it can be obtained:

$$f_{pk} = \left(\alpha_0 + \frac{1}{\sqrt{3}} \right) \sigma_{pk} \tag{9}$$

$$\left.\frac{\mathrm{d}\sigma_1}{\mathrm{d}\varepsilon_1}\right|_{\varepsilon_1=\varepsilon_{\mathrm{pk}}}=0 \tag{10}$$

Substitute the peak points (σ_{pk}, $\varepsilon_{\mathrm{pk}}$) of the stress-strain curve into equation (5):

$$\frac{\sigma_{\mathrm{pk}}}{E\varepsilon_{\mathrm{pk}}}=\exp\left[-\left(\frac{f_{\mathrm{pk}}}{f_0}\right)\right]^m \tag{11}$$

Take the logarithm of both sides of the equation:

$$\left(\frac{f_{\mathrm{pk}}}{f_0}\right)^m=\ln\left(\frac{E\varepsilon_{\mathrm{pk}}}{\sigma_{\mathrm{pk}}}\right) \tag{12}$$

Where f_{pk} is the micro-element strength corresponding to the peak strength of sandstone

Take the derivative of strain ε_1 on both sides of equation (5). Assuming that the micro-element strength is approximately linearly related to the strain ε_1, according to Equation (10), we can obtain :

$$\left(\frac{f_{\mathrm{pk}}}{f_0}\right)^m=\frac{1}{m} \tag{13}$$

Combining (11) and (12), the Weibull distribution parameters m and f_0 can be expressed :

$$m=\frac{1}{\ln\left(\frac{E_1\varepsilon_{\mathrm{pk}}}{\sigma_{\mathrm{pk}}}\right)} \tag{14}$$

$$f_0=f_{\mathrm{pk}}m^{\frac{1}{m}} \tag{15}$$

5.2 Damage variable under macroscopic prefabricated fissure

Define the initial damage variable D_{k} considering rocks with prefabricated fissures. Based on energy theory and fracture theory, the period from the initial loading to the failure of rocks is regarded as the storage and release of elastic energy. Ignoring other energy losses such as thermal energy and kinetic energy, the elastic energy of rocks with prefabricated fissures can be expressed as $U^{\mathrm{e}'}$ (Liu et al.,2016).

$$U^{\mathrm{e}'}=\left[\frac{\sigma_1^2}{2E_1\left(1-D_{\mathrm{k}}\right)}\right] \tag{16}$$

If the change in elastic energy is ΔU and the volume of the rock specimen is V, then ΔU can be expressed as:

$$\Delta U=U^{\mathrm{e}'}-U^{\mathrm{e}}=V\left[\frac{\sigma_1^2}{2E_1\left(1-D_{\mathrm{k}}\right)}-\frac{\sigma_1^2}{2E_1}\right] \tag{17}$$

Based on fracture theory (Xu et al.,2025), for the planar strain problem, the additional elastic energy increment U^{a} caused by the existence of cracks in an ideal elastic medium can be expressed as :

$$U^a=\int_0^{A_{\mathrm{c}}}G\mathrm{d}A_{\mathrm{c}}=\frac{1-\mu^2}{E_1}\int_0^{A_{\mathrm{c}}}\left(K_{\mathrm{I}}^2+K_{\mathrm{II}}^2\right)\mathrm{d}A_{\mathrm{c}} \tag{18}$$

Where A_{c} is the area of the prefabricated fracture, mm^2; μ is Poisson's ratio; K_{I} and K_{II} are the Type I and Type II stress intensity factors of the fissure tip wing crack.

Since both U^{a} in Equation (18) and ΔU in Equation (17) represent the changes in elastic energy caused by prefabricated fissures, then :

$$V\left[\frac{\sigma_1^2}{2E_1(1-D_k)}-\frac{\sigma_1^2}{2E_1}\right]=\frac{1-\mu^2}{E_1}\int_0^{A_c}\left(K_I^2+K_{II}^2\right)dA_c \tag{19}$$

From Equation (19), the damage variable D_k of the prefabricated fissured rock can be expressed :

$$D_k=1-\left[\frac{2(1-\mu^2)}{V\sigma_1^2}\int_0^{A_c}\left(K_I^2+K_{II}^2\right)dA_c+1\right]^{-1} \tag{20}$$

Let the prefabricated fissure angle be θ, then the normal stress component σ_a and the shear stress component τ_b on the fissure surface under uniaxial compression can be expressed as :

$$\begin{cases}\sigma_a(\sigma,\theta)=\sigma_1\cos^2\theta\\ \tau_b(\sigma,\theta)=\dfrac{\sigma_1}{2}\sin 2\theta\end{cases} \tag{21}$$

Where σ is the axial stress.

The sliding driving force τ_c on the fissure surface under uniaxial compression can be expressed as :

$$\tau_c=\begin{cases}0, & (\tan\theta<\tan\varphi_c)\\ \tau_b-\sigma_a\tan\varphi_c, & (\tan\theta\geq\tan\varphi_c)\end{cases} \tag{22}$$

Where φ_c is the friction angle of the fissure surface.

It can be seen from Table 3, the wing cracks initiated near the fissure tip are the main cause of sandstone failure. The wing cracks are caused by the tensile stress induced by the frictional sliding between the prefabricated fissure surfaces under axial pressure at the fissure tip (Fig. 13).

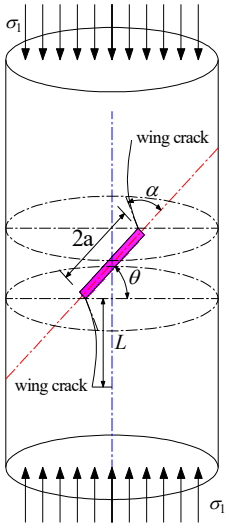


Fig.13. Schematic diagram of wing crack propagation.

The stress intensity factors of K_I type and K_{II} type for wing cracks can be expressed as :

$$\begin{cases}K_I=-\dfrac{2a\tau_c\sin\alpha}{\sqrt{\pi(l+l^*)}}+\sigma_a(\sigma,\alpha+\theta)\sqrt{\pi l}\\ K_{II}=-\dfrac{2a\tau_c\cos\alpha}{\sqrt{\pi(l+l^*)}}+\tau_b(\sigma,\alpha+\theta)\sqrt{\pi l}\end{cases} \tag{23}$$

Where a is the half-length of the prefabricated fissure, mm; l is the length of crack propagation, mm; α is the crack propagation angle of the wing. (Zhang et al.,2016) found that under uniaxial compressive loading, the wing cracks caused by non-through fissures propagate approximately in the direction of α=70.5° from the fissure tip, as shown in Fig. 13, along the direction of the maximum tensile stress. In this paper, α=70.5° is taken. To prevent the crack propagation length from being too small, l^*=0.27a is introduced so that when l = 0, K_I and K_{II} are non-singular(Pan et

al.,2022) . Considering the critical value of the wing crack propagation state, when $l = 0$, the stress intensity factors can be expressed as :

$$\begin{cases} K_{\mathrm{I}} = -\dfrac{2a\tau_{\mathrm{c}}\sin\alpha}{\sqrt{\pi l^{*}}} \\ K_{\mathrm{II}} = -\dfrac{2a\tau_{\mathrm{c}}\cos\alpha}{\sqrt{\pi l^{*}}} \end{cases} \tag{24}$$

When $l = 0$, the wing crack is in the critical state of initiation. Substituting Equation (24) into equation (20), the initial damage variable D_{k} can be obtained, which characterizes the degree of deterioration of the initial mechanical properties of the rock caused by the prefabricated fissure before macroscopic failure. Therefore, the initial damage variable D_{k} expression for rocks with prefabricated fissures can be expressed as :

$$D_{\mathrm{k}} = 1 - \left\{ 1 + \left[\frac{29.63a^{2}b\cos^{2}\theta\left(1-\mu^{2}\right)\left(\sin\theta - \cos\theta\tan\varphi_{\mathrm{c}}\right)^{2}}{\pi V} \right] \right\}^{-1} \tag{25}$$

Where b is the width of the prefabricated fissure.

5.3 CFRP constraint modification

After CFRP constraint is applied to prefabricated fractured sandstone, the damage variables need to take into account the obstruction of fracture propagation and the effect of CFRP constraint. The the effect of CFRP constraint is equivalent to passive confining pressure, and the constraint stress increases with the radial expansion and can inhibit the opening and expansion of fissures. According to the conclusion of Jiang et al. (Jiang et al.,2007), the constraint stress of CFRP can be expressed by Equation (26) :

$$\sigma_{\mathrm{CFRP}} = \frac{2t_{\mathrm{CFRP}}E_{\mathrm{CFRP}}\varepsilon_{\mathrm{CFRP}}}{R} \tag{26}$$

Where σ_{CFRP} is the constraint stress of CFRP, MPa; t_{CFRP} is the thickness of CFRP, mm; R is the diameter of the specimen; E_{CFRP} is the elastic modulus, GPa; $\varepsilon_{\mathrm{CFRP}}$ is the tensile strain of CFRP, %.

In Equation (26), σ_{CFRP} is an unsteady variable, which is caused by the radial expansion deformation of the rock. According to the generalized Hooke's law, if CFRP and rock undergo co-deformation under uniaxial compression, then the tensile strain of CFRP is equal to the radial strain. According to the research results of Lam et al.(Lik Lam et al.,2003), the constraint stiffness coefficient η of CFRP can be expressed by equation (27) :

$$\eta = \frac{\sigma_{\mathrm{CFRP}}}{\sigma_{1}} \tag{27}$$

In fracture mechanics, the general expression of the stress intensity factor can be expressed as:

$$K = Y\sigma\sqrt{\pi a} \tag{28}$$

CFRP can inhibit crack opening, and the stress intensity factor K_{I} needs to be modified. The CFRP constraint coefficient β is introduced to modify the stress intensity factor K_{I} , and the modified the stress intensity factor K_{I} can be expressed as :

$$K_{\mathrm{I}}^{\mathrm{e}} = \max\left\{0,\quad K_{\mathrm{I}} - \beta(\sigma_{1}\eta)\sqrt{\pi a}\right\} \tag{29}$$

Where $K_{\mathrm{I}}^{\mathrm{e}}$ is the modified stress intensity factor K_{I}; β is the constraint coefficient of CFRP.

Substituting the modified stress intensity factor $K_{\mathrm{I}}^{\mathrm{e}}$ into equation (20), the damage variable

D_k of the rock with prefabricated fissures, which is subject to CFRP constraint modification, can be obtained :

$$D_k = 1 - \left\{ 1 + \lambda - \frac{15.4a^2 b\cos\theta\left(1-\mu^2\right)M\beta\sin\alpha}{V} + \frac{2\pi a^2 b\left(1-\mu^2\right)\beta^2\eta^2}{V} \right\}^{-1} \tag{30}$$

In Equation (30), M and λ can be expressed by equation (31) as :

$$\begin{cases} M = \sin\theta - \cos\theta\tan\varphi_c \\ \lambda = \dfrac{29.63a^2 b\cos\theta\left(1-\mu^2\right)\left(\sin\theta - \cos\theta\tan\varphi\right)^2}{\pi V} \end{cases} \tag{31}$$

According to Hooke's law, the stress-strain relationship of rocks under uniaxial compression can be expressed as :

$$\varepsilon = \frac{\sigma}{E} \tag{32}$$

For rocks with prefabricated fissures, the damage during uniaxial compression includes microscopic damage caused by loads and initial damage caused by prefabricated fissures. Based on the strain equivalence assumption, the strain of fissured sandstone constrained by CFRP can be expressed as :

$$\varepsilon_1 = \frac{\sigma}{E_1} = \frac{\sigma}{E_k} + \frac{\sigma}{E_m} - \frac{\sigma}{E_0} \tag{33}$$

Where E_1 is the elastic modulus of the macroscopic and microscopic coupling damage of sandstone during the loading process, GPa; E_k is the elastic modulus of prefabricated fissured sandstone after CFRP constraint modification; E_m is the micro-damage elastic modulus under load, GPa; E_0 is the initial elastic modulus, GPa. The three elastic modulus can be respectively expressed as :

$$\begin{cases} E_1 = E_0\left(1-D\right) \\ E_m = E_0\left(1-D_m\right) \\ E_k = E_0\left(1-D_k\right) \end{cases} \tag{34}$$

Substitute equation (34) into equation (33) :

$$D = 1 - \frac{\left(1-D_m\right)\left(1-D_k\right)}{1+D_m D_k} \tag{35}$$

Where D_1 is the macroscopic and microscopic coupling damage variable; D_m is the micro-damage variable under load; D_k is the damage variable with prefabricated fissures after CFRP constraint modification.

In conclusion, it can be concluded that the stress-strain constitutive relationship of sandstone with prefabricated fissures considering CFRP constraint modification can be expressed as :

$$\sigma_1 = \frac{E_0\varepsilon\exp\left[-\left(\dfrac{f}{f_0}\right)^m\right]\left\{1+\lambda-\dfrac{15.4a^2 b\cos\theta\left(1-\mu^2\right)M\beta\sin\alpha}{V}+\dfrac{2\pi a^2 b\left(1-\mu^2\right)\beta^2\eta^2}{V}\right\}^{-1}}{1+\left(1-\exp\left[-\left(\dfrac{f}{f_0}\right)^m\right]\right)\left(1-\left\{1+\lambda-\dfrac{15.4a^2 b\cos\theta\left(1-\mu^2\right)M\beta\sin\alpha}{V}+\dfrac{2\pi a^2 b\left(1-\mu^2\right)\beta^2\eta^2}{V}\right\}^{-1}\right)} \tag{36}$$

5.4 Model verification

According to Equation (36), the parameters include the half-length of the fissure a, the width

of the fissure b, the volume of the specimen V, the diameter of the specimen R, and the fissure angle θ, which can be directly obtained through sandstone specimen. The CFRP thickness t_{CFRP} and elastic modulus E_{CFRP} can be obtained through the CFRP producer. The internal friction Angle φ, initial modulus E_0, Poisson's ratio μ, The stress σ_1 and strain ε_1 of sandstone can be obtained through uniaxial compression tests. The Weibull distribution parameters m and f_0 can be calculated from the stress-strain curve of the sandstone. The CFRP constraint coefficient β can be obtained through fitting of the uniaxial test data.

Based on the uniaxial compression test of fissured sandstone constrained by CFRP, the damage constitutive model in this paper is verified. The comparison results of the model curve and the test curve are shown in Fig. 14. Under different test conditions, the damage constitutive model of sandstone with prefabricated fissures in this paper considering the constraint modification of CFRP can basically describe the changing trend of the test curves. In the pre-peak stage, the test curve basically coincides with the model curve, with a high degree of agreement. However, in the post-peak stage, the test curve deviates from the model curve, but it can basically describe the entire loading failure process of CFRP-constrained fissured sandstone. The comparison results verified the accuracy and rationality of the damage constitutive model of sandstone with prefabricated fissures in this paper considering the modification of CFRP constraints.

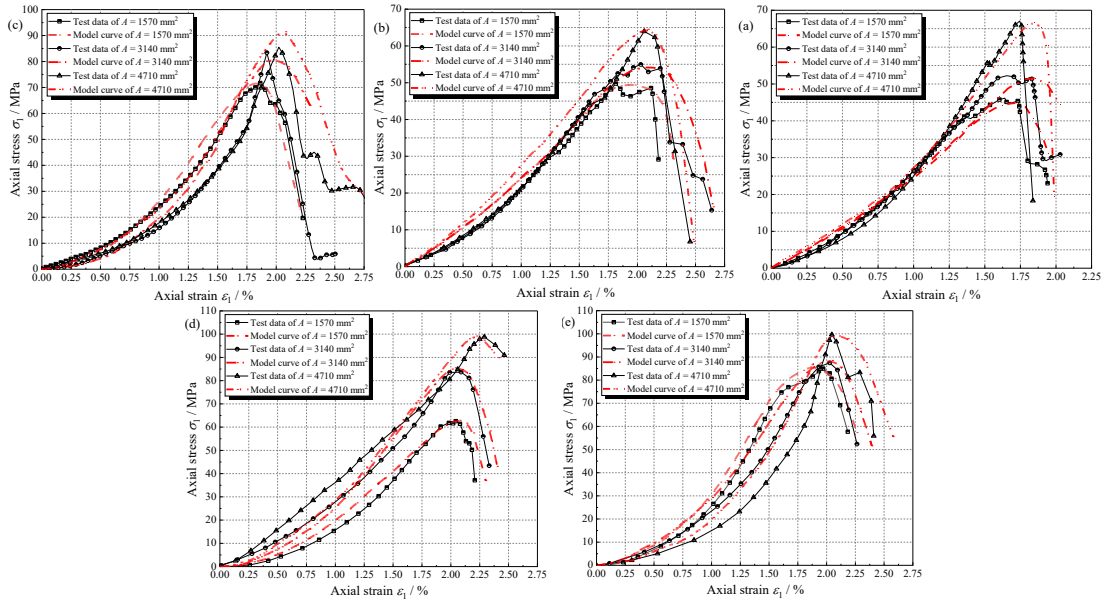


Fig.14. Model verification. (a) θ=0°; (b) θ=30°; (c) θ=45°; (d) θ=60°; (e) θ=90°.

Fig. 15 shows the comparison results of the curves of the models with CFRP constraint modification and without CFRP constraint modification. Both model curves can describe the changing trend of the test curve. In the pre-peak stage, both model curves are relatively close to the test curves. Among them, the model curve considering CFRP constraint modification is slightly better in agreement with the test curve than the model curve not considering CFRP modification. In the post-peak stage, the consistency between the model considering CFRP constraint modification and the test data is significantly improved, verifying the rationality of the damage constitutive model of fissured sandstone considering CFRP constraint modification proposed in this paper.

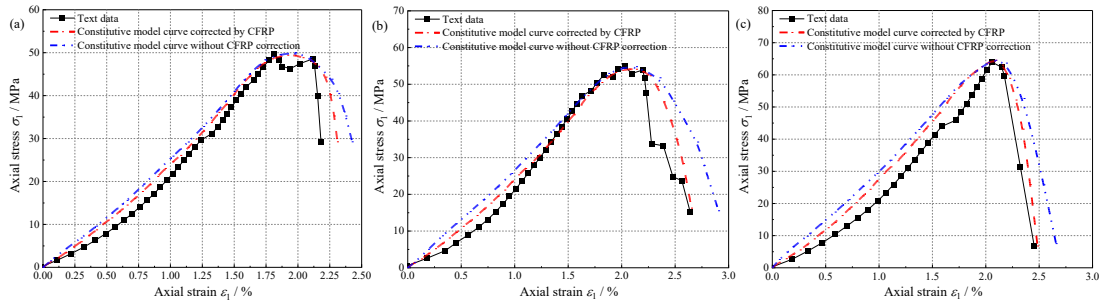


Fig.15. Model verification. (a) A=1570mm^2; (b) A=3140mm^2; (c) A=4710mm^2.

To further verify the accuracy of the model in this paper, the test results of Zhou et al. (Zhou et al.,2024) are cited and plotted together with the damage constitutive model curve in this paper in Fig. 16. The damage constitutive model curve of fissured sandstone considering CFRP constraint modification proposed in this paper is basically consistent with the test results in the literature, further verifying the accuracy of the model. It indicates that the damage constitutive model in this paper can predict the co-deformation and failure characteristics of the surrounding rock and support system, and has engineering application value.

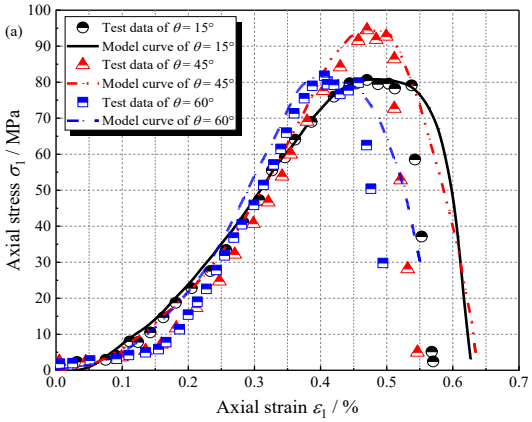


Fig.16. Model verification.

6. Discussion

Fig. 17 shows a schematic diagram of the damage mechanism of fissured sandstone under the constraint of CFRP. Under unconstrained conditions, the sandstone undergoes radial expansion during axial compression, resulting in stress concentration at the prefabricated fissure tips and further intensifying the expansion and penetration of the cracks. After the circumferential constraint is applied, CFRP provides a radial passive confining pressure opposite to the direction of the tensile stress, which suppresses the deformation of the specimen and thereby alters the stress state of the fissured sandstone. This transformation of the stress state increases the internal frictional resistance of the rock, inhibits the sliding and opening of cracks, and macroscopically manifested as an improvement in the ductility of the material and a slowdown in the rate of damage evolution, effectively suppressing the damage development of fissured rock mass.

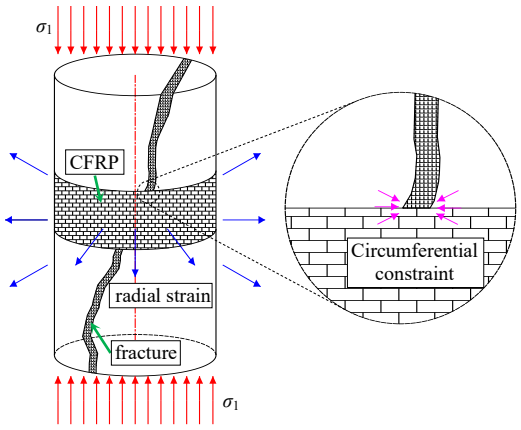


Fig.17. Failure mechanism of CFRP circumferential constrained fissured sandstone.

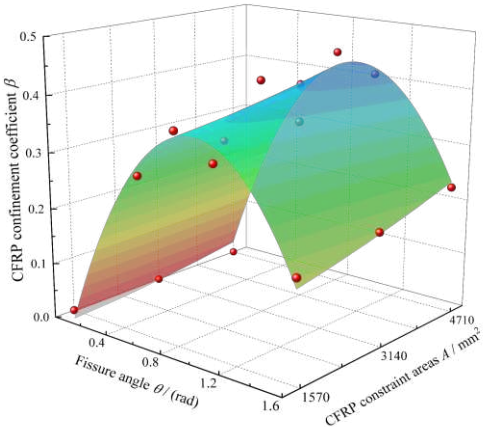


Fig.18. Relationship between the CFRP confinement coefficient with the fissure angle and constraint area.

In the damage constitutive model of this paper, the CFRP constraint coefficient β is introduced, which represents the effective degree of converting the CFRP constraint stress into suppressing the opening of the fissure tip. Essentially, it is the conversion efficiency coefficient between the macroscopic constraint force and the microcrack closure effect, and is affected by the fissure angle and constraint area. The β can be obtained through fitting. Fig. 18 shows the relationship between the CFRP constraint coefficient β, and the constraint area A and the fissure angle θ. There is a correlation between the CFRP constraint coefficient β and the constraint area A and the fissure angle θ. As the constraint area A gradually increases, the CFRP constraint coefficient β also increases, and its inhibitory effect on crack opening becomes stronger. As the fissure angle θ gradually increases, the CFRP constraint coefficient β shows a trend of first increasing and then decreasing, and taking the maximum value at the fissure angle of θ=45°. The data fitting reveals that the CFRP constraint coefficient β has a relationship with the constraint area A and the fissure angle θ that satisfies Equation (37) :

$$\beta = 0.5616 + 0.8287\theta + 0.000036A + 0.0232\theta^2 + 0.000056A^2 + 0.000097A\theta, \quad \left(R^2 = 9829\right) \quad (37)$$

The fitting results reveal that there is a strong correlation between the CFRP constraint coefficient β and the constraint area A as well as the fissure angle θ. When the CFRP constraint area A is relatively small, the effective compressive stress distribution generated by the constraint stress field within the rock is uneven, resulting in a smaller constraint coefficient β value. When the CFRP constraint area A is relatively large, its constraint can act more evenly on the prefabricated fissure tip, thereby suppressing the propagation of $K_I$tensioning cracks and causing the CFRP constraint coefficient β to be larger. It is indicated that in the process of deep roadway support, the density of the support structure (such as the spacing of anchor rods) directly determines the size of the constraint coefficient, which in turn affects the overall bearing capacity of the surrounding rock.

7. Conclusions

Aiming at the problem of coordinated deformation and failure of the advanced support structure of deep roadways and the fissured rock mass above, taking the transportation roadway of the 40101 mining face of Gaojialiang Coal Mine in Ordos as the engineering background, the CFRP is adopted to approximately simulate the flexible support structure formed by the surrounding rock and the advanced support together. The mechanical properties, failure modes

and energy damage evolution laws of sandstone under different CFRP constraint areas and fissure angles are analyzed through uniaxial compression tests. The specific conclusions are as follows :

(1) As the CFRP constraint area gradually increases, the peak strength, elastic modulus and peak strain of fissured sandstone all show a gradually increasing trend, the Poisson's ratio gradually decreases, and the failure mode gradually changes from brittle splitting failure to ductile shear failure. The influence of fissure angle on mechanical parameters shows obvious anisotropy. The peak strength, elastic modulus and peak strain all change with the fissure angle in a pattern of "first decreasing and then increasing", with the minimum value occurring when the fissure angle θ=45°. The Poisson's ratio monotonically increases with the fissure angle.

(2) Under different CFRP constraint areas, as the axial load gradually increases, the proportion of dissipated energy gradually increases. As the CFRP constraint area gradually increases, the total energy and elastic energy corresponding to the same axial strain gradually increase, while the dissipated energy gradually decreases. This indicates that the CFRP constraint effect enhances the energy storage capacity of fissured sandstone, delays the critical point for the conversion of elastic energy to dissipated energy, effectively inhibits the development of sandstone cracks, and significantly increases the initial stress level of damage.

(3) As the CFRP constraint area gradually increases, the CFRP constraint coefficient β gradually increases. As the fissure angle gradually increases, the CFRP constraint coefficient β shows a trend of first increasing and then decreasing, and taking the maximum value at the fissure angle of θ=45°. Based on fracture mechanics and statistical damage theory, the stress intensity factor K_I at the tip of sandstone fissures is modified by the CFRP constraint coefficient β, and a damage constitutive model of sandstone with prefabricated fissures considering the modification of CFRP constraints is established. The accuracy and rationality of the model in this paper are verified based on the test results.

Authorship contribution Conceptualization: Lei Chen ; Data curation: Lei Chen , Taiyu Liu ; Formal analysis: Shuguang Zhang and Jiaxu Jin; Investigation: Jupeng Tang and Baoxin Jia ; Methodology: Lei Chen and Taiyu Liu; Writing-original draf: Lei Chen and Taiyu Liu; Writing-review & editing: Jiashun Liu and Lei Chen:.

Declaration of competing interest The authors declare that they have no known competing financial interests or personal relationships that could have appeared to influence the work reported in this paper.

Availability of data and materials The data and materials that has been used is confidential.

Declarations

Ethies approval and consent to participate The authors declare that the research and relatedactivities in this article do not involve human participants or ethical issues.

Consent to publish The authors agree to publication in the Geomechanics and Geophysics for Geo-Energy and Geo-Resources and also to publication ofthe article in English by Springer in Springer 'scorresponding English-language journal.

References

Liu H, Zhao JH, Ma Q et al (2026) Degradation mechanism of microstructure of residual coal pillars during highly mineralized mine-water storage in coal mine goaf. Underground Space 26(1): 479-497.

DOI:10.1016/j.undsp.2025.10.001.

Ling K,Sun J, Han JZ, Liu DQ(2024) Experimental study on the failure behavior of rockburst induced by a dynamic disturbance in the circular chamber for deep underground engineering. Engineering Failure Analysis 164(1): 108708. DOI: 10.1016/j.engfailanal.2024.108708.

Deng P, Wei HL, Du JT, Zhang C, Chen RP (2026) Seismic fragility analysis of deep underground structures based on fault-to-structure earthquake simulation. Soil Dynamics and Earthquake Engineering 200(Part A): 109800. DOI: 10.1016/j.soildyn.2025.109800.

Zhang BJ, Tan JS, Zhao JP, Zhou ZL (2025) Research on the deformation mechanisms and control systems for tunnels subjected to squeezing in weak surrounding rock. Tunnelling and Underground Space Technology, 165(1): 106914. DOI: 10.1016/j.tust.2025.106914.

Liu HJ, He C,Yue T, Xu GW et al (2025) Stability analysis of surrounding rock in large-section tunnels considering the random distribution of rock mass mechanical parameters and joint fractures. Engineering Failure Analysis 182 (Part A): 110039. DOI: 10.1016/j.engfailanal.2025.110039.

Sun BJ, Mei YC, Li WT et al (2024) Experimental study on the deformation and failure mode of surrounding rocks of a tunnel in a jointed rock mass. Engineering Failure Analysis 163(Part A): 108470. DOI: 10.1016/j.engfailanal.2024.108470.

Xie SR, Ren YX, Chen DD et al (2025) A case study on coordinated asymmetric support-relief control for roadway surrounding rock under multiple dynamic pressures in thick coal seams. Engineering Failure Analysis, 179(1): 109821. DOI: 10.1016/j.engfailanal.2025.109821.

Zhang CC, Wu HN, Chen RP et al (2026) Interaction mechanism between primary support and surrounding rock in shallow tunnels considering time effects. Tunnelling and Underground Space Technology 169(1): 107308. DOI: 10.1016/j.tust.2025.107308.

Pi S, Wang MN, Luo X et al (2026) Study and application of energy-dissipating yielding support for large deformation in hard rock tunnel subjected to extremely high geostress. Tunnelling and Underground Space Technology 169(1): 107293. DOI: 10.1016/j.tust.2025.107293.

Zhang SG, Yang JF, Li YM et al (2022) Research on Rheological Energy Characteristics of Fractured Sandstone Strengthened with CFRP. Sustainability 14(23): 16212. DOI: 10.3390/su142316212.

Liu MY, Tian J, Zhao J, Sun YP et al (2025) Seismic performance of CFRP-strengthened steel fiber reinforced concrete composite columns: Experimental, numerical and theoretical analyses. Construction and Building Materials 505(1): 144692. DOI: 10.1016/j.conbuildmat.2025.144692.

Zhou YJ, Wang MS, Lian YJ, Yang N et al (2025) Fatigue and corrosion interaction: Performance evolution mechanisms in reinforced concrete beams strengthened with CFRP anchorage system, Construction and Building Materials 496(1): 143784. DOI: 10.1016/j.conbuildmat.2025.143784.

Wang ZX, Chen XD, Shi ZY, Wu WW et al (2025) Flexural performance and damage evolution of coral sand reinforced concrete beams strengthened with CFRP sheets: A machine learning-based analysis,Engineering Structures,A machine learning-based analysis. Engineering Structures 343(Part C): 121155. DOI: 10.1016/j.engstruct.2025.121155.

Willy HZ, Cheng HY, Chung CH (2025) Flexural and shear strengthening of lightly reinforced concrete beams using CFRP bars and UHPC overlays. Case Studies in Construction Materials 22(1): e04666. DOI: 10.1016/j.cscm.2025.e04666.

Liu JD, Fan XQ, Zou L,Shi CY (2025) Effect of different CFRP strengthening methods on fracture parameters of concrete beam. Engineering Fracture Mechanics 314(1): 110748. DOI: 10.1016/j.engfracmech.2024.110748.

Zhang W, Yang XZ, Lin JW, Lin BQ, Huang YQ (2024) Experimental and numerical study on the torsional behavior of rectangular hollow reinforced concrete columns strengthened By CFRP. Structures 70(1): 107690.

DOI: 10.1016/j.istruc.2024.107690.

Zhang SH, Jiang YJ, Luan HJ et al (2024) Study on Shear Mechanical Characteristics of Rock Joints Under Different Anchorage Lengths. Rock Mechanics and Rock Engineering 57(12): 9959–9981. DOI: 10.1007/s00603-024-04075-2.

Wei Y, Lai XP, Pei ZH et al (2024) Experimental and Numerical Study on the Anchoring Mechanism of an Anchor Bolt Considering its Lateral Restraint Effect. Rock Mechanics and Rock Engineering 57(12): 9617–9633. DOI: 10.1007/s00603-024-03981-9.

Wang Q, Xin ZX, Jiang B et al (2023) Mechanical properties of rocks anchored by constant resistance energy-absorbing material. Journal of Central South University 30(11): 3361–3373. DOI: 10.1007/s11771-023-5456-8.

Ning JG, Zhang ZH, Wang J, Wang L, Shi XS, Hu SC (2025) Study on the effect of static fissure on the stress field of anchored rock beam and axial force of bolt. Engineering Failure Analysis 174(1): 109514. DOI: 10.1016/j.engfailanal.2025.109514.

Su HJ, Zhang LQ, Yu LY, Jiang Y et al (2024) Analysis of the fracture response of anchored rock under three-point bending from experimental and numerical perspectives. Theoretical and Applied Fracture Mechanics 134(Part A): 104692. DOI: 10.1016/j.tafmec.2024.104692.

Song YM, Fan JY,An D et al (2026). Study on surrounding rock control performance of pile-anchored energy-absorbing hydraulic support in rockburst roadways of kilometer-deep mines. Results in Engineering, 29(1): 108430. DOI: 10.1016/j.rineng.2025.108430.

Jorge Terron-Almenara, Karl Gunnar Holter, et al (2025) Permanent tunnel support with reinforced shotcrete arches and forepoling in over-consolidated till and weathered rock. A case study based on the construction of the Bergås tunnel, Norway. Tunnelling and Underground Space Technology 157(1): 106256. DOI: 10.1016/j.tust.2024.106256.

Chen L, Lu PP, Zhang SG (2022) Failure Mechanism and Energy Damage Evolution of Deep Sandstone Anchored by Carbon Fiber. KSCE Journal of Civil Engineering 26(4): 1929–1949. DOI: 10.1007/s12205-022-1127-9.

Gu LJ, Zhu GQ, Li SJ et al (2026) Strain energy calculation and differential evolution in deep hard rocks under different true triaxial unloading paths with cyclic loading. International Journal of Rock Mechanics and Mining Sciences 197(1): 106343. DOI: 10.1016/j.ijrmms.2025.106343.

Zhang K, Wang W, Cao YJ,Duan XL, et al (2025) Energy-damage analysis of rock brittleness incorporating complete stress-strain behavior and effects of confining pressure and lithology. Journal of Rock Mechanics and Geotechnical Engineering 17(12): 7993–8016. DOI: 10.1016/j.jrmge.2025.06.040.

WEIBULL W (1951). A statistical distribution function of wide applicability. Journal of Applied Mechanics 18(3): 293−297. DOI: 10.1115/1.4010337.

Lemaitre J (2012). A course on damage mechanics. Berlin: Springer Science & Business Media. DOI: 10.1007/978-3-662-02761-5.

Alcazar E, Paulino G H (2026) Topology optimization for pressure-dependent elastoplastic structures considering a smooth hyperbolic approximation of the Drucker-Prager yield criterion. Computer Methods in Applied Mechanics and Engineering 449(Part B): 118446. DOI: 10.1016/j.cma.2025.118446.

Liu HY, Su TM (2016) A dynamic damage constitutive model for a rock mass with non-persistent joints under uniaxial compression. Mechanics Research Communications 77(1): 12–20. DOI: 10.1016/j.mechrescom.2016.08.006.

Xu W, Shi CN, Liu B (2025) A physical mode partition and VCCT for mixed mode crack. Engineering Fracture Mechanics 330: 111707. DOI: 10.1016/j.engfracmech.2025.111707.

Zhang LM, Zhang H, Liu HY (2016) A damage constitutive model for rock mass with non-persistently closed

joints under uniaxial compression load. Coal Geology and Exploration 44(1):79-84. DOI:1001-1986(2016)01-0079-06. (in Chinese)

Pan JL, Cai MF, Li P (2022) A damage constitutive model of rock-like materials containing a single crack under the action of chemical corrosion and uniaxial compression. Journal of Central South University 29(2): 486-498. DOI:10.1007/s11771-022-4949-1.

Jiang T, Teng JG (2007) Analysis-oriented stress–strain models for FRP–confined concrete. Engineering Structures 29(11): 2968–2986. DOI: 10.1016/j.engstruct.2007.01.010.

Lik Lam, Teng JG (2003) Design-oriented stress–strain model for FRP-confined concrete. Construction and Building Materials 17(7): 471–489. DOI: 10.1016/S0950-0618(03)00045-X.

Hu QT, Yu CJ, Li QG (2025) Experimental study on the macro- and meso-damage and failure characteristics of fractured sandstone under uniaxial compression. Journal of Experimental Mechanics 40(1): 49–60. DOI: 10.7520/1001-4888-23-153.

Zhou T, Chen CP, Fang YL et al (2024). Effect of CFRP-wrapping on the mechanical and failure behavior of sandstone specimen containing a single flaw under compression. Construction and Building Materials 442(1):137575. DOI:10.1016/j.conbuildmat.2024.137575.